North Atlantic hotspot-ridge interaction near Jan Mayen Island

L.J. Elkins[1,2]*, C. Hamelin[3]*, J. Blichert-Toft[4],
S.R. Scott[5], K.W.W. Sims[5], I.A. Yeo[6],
C.W. Devey[6], R.B. Pedersen[3]

OPEN ACCESS

Abstract

At slow to ultraslow spreading rates along mid-ocean ridges, thicker lithosphere typically impedes magma generation and tectonic extension can play a more significant role in crustal production (Dick *et al.*, 2003). The source of anomalously high magma supply thus remains unclear along ridges with ultraslow-spreading rates adjacent to Jan Mayen Island in the North Atlantic (Neumann and Schilling, 1984; Mertz *et al.*, 1991; Haase *et al.*, 1996; Schilling *et al.*, 1999; Trønnes *et al.*, 1999; Mertz *et al.*, 2004; Blichert-Toft *et al.*, 2005; Debaille *et al.*, 2009). Here we show that Jan Mayen volcanism is likely the surface expression of a small mantle plume, which exerts significant influence on nearby mid-ocean ridge tectonics and volcanism. Progressive dilution of Jan Mayen geochemical signatures with distance from the hotspot is observed in lava samples from the immediately adjacent Mohns Ridge, and morphological indicators of enhanced magma supply are observed on both the Mohns Ridge and the nearby Kolbeinsey Ridge, which additionally locally overlies a highly heterogeneous, eclogite-bearing mantle source. These morphological and geochemical influences underscore the importance of heterogeneous mantle sources in modifying melt supply and thus the local expression of tectonic boundaries.

1   Department of Geology, Bryn Mawr College, 101 North Merion Avenue, Bryn Mawr, Pennsylvania 19010, USA
2   Department of Earth and Atmospheric Sciences, University of Nebraska Lincoln, Lincoln, NE 68588, USA
3   Center for Geobiology, University of Bergen, Allegaten 41 5007, Bergen, Norway
*   Corresponding and first authors (email: lelkins@unl.edu, Cedric.Hamelin@uib.no)
4   Laboratoire de Géologie de Lyon, Ecole Normale Superieure de Lyon, 46 Allée d'Italie, 69007 Lyon, France
5   Department of Geology and Geophysics, University of Wyoming, Laramie, Wyoming 82071, USA
6   GEOMAR, Helmholtz Center for Ocean Research Kiel, Wischhofstraße 1-3 24148, Kiel, Germany

Letter

The normal accretion process along divergent plate boundaries can be notably altered in hotspot-ridge interaction settings, where elevated mantle temperature anomalies enhance mantle melting, generating unusually thick oceanic crust (*e.g.,* Schilling *et al.*, 1985; Schilling, 1991; Gale *et al.*, 2013, 2014). Jan Mayen and its immediate environs in the North Atlantic (Fig. 1) include an intraplate, volcanically-active island or hotspot (Jan Mayen Island), positioned at the northern terminus of a small, rifted microcontinent (Jan Mayen Ridge; Johnson and Heezen, 1967; Kodaira *et al.*, 1997; Gaina *et al.*, 2009) and adjacent to two second-order ultraslow-spreading (Dick *et al.,* 2003) ridge segments, the Northern Kolbeinsey Ridge (NKR) and Southern Mohns Ridge (SMR), and the Jan Mayen Fracture Zone, a major fracture zone with ~200 km of transform offset. Although different in key ways, broad geochemical similarities between Jan Mayen Island and Icelandic lavas have suggested the influence of a mantle plume (either a unique Jan Mayen plume or emplaced Icelandic material) on mantle melting beneath Jan Mayen Island (Schilling *et al.*, 1999; Trønnes *et al.*, 1999; Debaille *et al.*, 2009). The absence of a clear hotspot track has led to conflicting, alternate interpretations for Jan Mayen's high magma production rate and enriched chemistry (Imsland, 1986; Maaløe *et al.*, 1986; Thy *et al.*, 1991): cold edge effects near the fracture zone (Mertz *et al.*, 1991; Haase *et al.*, 1996), variably melting source heterogeneities (Mertz *et al.*, 1991; Haase *et al.*, 2003; Mertz *et al.*, 2004), upwelling along a mantle chemical discontinuity (Blichert-Toft *et al.*, 2005), or a locally wet mantle (Haase *et al.*, 2003; Mertz *et al.*, 2004). Jan Mayen thus presents a useful case study for 1) exploring the mechanisms by which hotspot volcanism can influence ultraslow-spreading ridge morphology, behaviour, and volcanism, 2) determining the relationships between hotspot volcanism and ambient variations in mantle geochemistry, and 3) exploring the disputed origins of local volcanic activity.

For this study, we present comprehensive geochemical analyses (major and trace element concentrations and $^{87}Sr/^{86}Sr$, $^{143}Nd/^{144}Nd$, $^{176}Hf/^{177}Hf$, $^{206}Pb/^{204}Pb$, $^{207}Pb/^{204}Pb$, and $^{208}Pb/^{204}Pb$ compositions) for a suite of submarine volcanic rocks from the NKR, the SMR, and Jan Mayen Island (Tables 1, S-1, S-2, S-3). These geochemical results are interpreted in the context of an enhanced geologic perspective, thanks to new high-resolution bathymetry of the volcanic and tectonic submarine morphology (Fig. 1). All submarine samples were retrieved during recent research cruises in combination with new multibeam bathymetry (Pedersen *et al.*, 2010; Devey, 2012). Three additional, subaerial alkali basalts from Jan Mayen Island are included for literature comparison (Maaløe *et al.*, 1986).

In agreement with previous work (Trønnes *et al.*, 1999; Debaille *et al.*, 2009), Jan Mayen Island lavas are "enriched" with relatively high $^{87}Sr/^{86}Sr$, $^{206}Pb/^{204}Pb$, $^{207}Pb/^{204}Pb$, and $^{208}Pb/^{204}Pb$ and low ε_{Hf} and ε_{Nd} (*e.g.,* $^{87}Sr/^{86}Sr$ = 0.703368-0.703490) (Table 1), and with trace element abundances resembling other ocean island basalts (Table S-2, Fig. S-1). While similar, Jan Mayen area lavas exhibit a
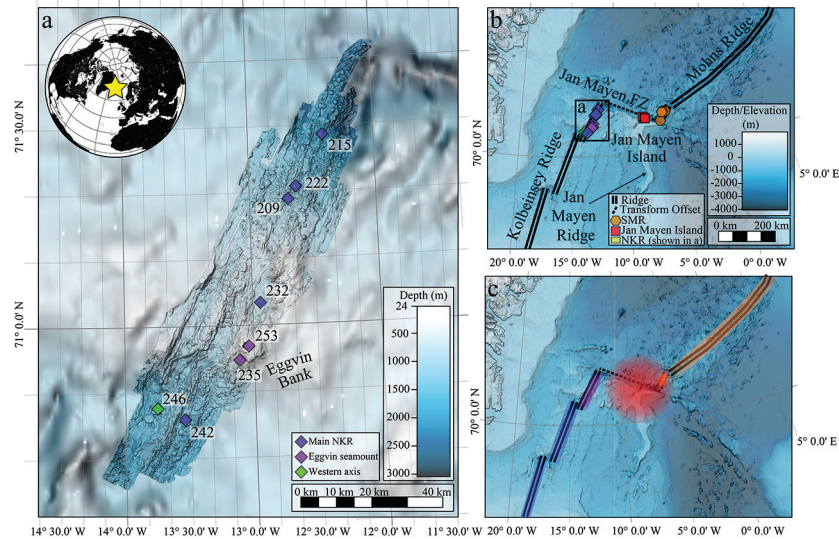
Figure 1 **(a)** Multibeam bathymetric map of the NKR, showing the Eggvin Bank and numbered dredge locations for samples analysed in this study. **(b)** Regional bathymetric map showing distribution of labelled seafloor features and Jan Mayen Island, with sample locations for this study from Jan Mayen Island (red), NKR (colours as in panel a), and SMR (orange). **(c)** Map with highlighted areas showing the proposed zones of underlying mantle melt generation and migration (blue: Kolbeinsey-type; purple: Eggvin-type; orange: Mohns-type; and red circle: Jan Mayen-type mantle).

distinct geochemical composition from Icelandic lavas (*e.g.,* higher $^{87}Sr/^{86}Sr$ and Pb isotope ratios, lower $^{143}Nd/^{144}Nd$ and $^{176}Hf/^{177}Hf$, normal MORB $^3He/^4He$, and distinct $^{187}Os/^{188}Os$ on Jan Mayen Island; Schilling *et al.*, 1999; Hanan *et al.*, 2000; Blichert-Toft *et al.*, 2005; Debaille *et al.*, 2009), suggesting an enriched source discrete from the Icelandic hotspot source, possibly entraining subcontinental lithospheric mantle (SCLM) (Debaille *et al.*, 2009). The submarine samples from Jan Mayen Island appear relatively evolved compared to the most magnesian subaerial samples of this study (MgO = 5.1-6.45 vs. 10.6-11.1 wt. %; Table S-3), but as previously observed, there are no systematic trace element or isotopic variations correlating with differentiation, arguing against detectable crustal assimilation (Trønnes *et al.*, 1999) (Tables 1, S-2, S-3).

The Mohns Ridge is an ultraslow-spreading ridge (17 mm yr^{-1} full-spreading rate; Mosar *et al.*, 2002; Dick *et al.*, 2003) north of Jan Mayen Island with relatively thin crust (~4 km; Klingelhofer *et al.*, 2000; Okino *et al.*, 2002; Ljones *et al.*, 2004; Kandilarov *et al.*, 2008) and mainly characterised by highly oblique spreading expressed as a series of *en echelon* rift basins (Géli *et al.*, 2012). In contrast, its southern segment (the SMR) has an orthogonal spreading direction and irregular off-axis crustal morphology, with a shallower ridge axis and thicker

crust (~10 km; Kandilarov *et al.*, 2012) (Fig. 1). Recent mapping indicates the presence of large, partly eroded volcanic structures, often bisected by faulting (Pedersen *et al.*, 2010). We interpret these structural and morphological characteristics as indicative of magma supply considerably higher than along the rest of the Mohns Ridge, possibly reflecting the influence of a nearby mantle plume associated with enhanced melt production.

Table 1 Radiogenic isotope compositions measured by ICP-MS*.

Sample	Location**	$^{87}Sr/^{86}Sr$	$^{176}Hf/^{177}Hf$	$^{143}Nd/^{144}Nd$	$^{206}Pb/^{204}Pb$	$^{207}Pb/^{204}Pb$	$^{208}Pb/^{204}Pb$
Submarine samples:							
POS436 242DR-2b[a]	NKR	0.703151(5)	0.283175(5)	0.513006(6)	18.8926	15.5093	38.6157
POS436 246DR-2[a]	NKR	0.702961(6)	0.283255(4)	0.513083(5)	18.4553	15.4547	38.0857
POS436 235DR-1a[a]	NKR	0.703187(5)	0.283177(4)	0.513008(5)	18.8756	15.5177	38.5990
POS436 253DR-E2[a]	NKR	0.703195(7)	0.283175(4)	0.513015(5)	18.8899	15.5211	38.6184
POS436 253DR-6[a]	NKR	0.703203(7)	0.283183(4)	0.513019(5)	18.8881	15.5185	38.6109
POS436 232DR-1[a]	NKR	0.703047(7)	0.283217(4)	0.513044(5)	18.7881	15.5004	38.4908
POS436 209DR-2a[a]	NKR	0.703034(6)	0.283231(4)	0.513051(6)	18.7699	15.5003	38.4689
POS436 222DR-1[a]	NKR	0.703040(7)	0.283217(4)	0.513043(6)	18.8150	15.5047	38.5277
POS436 215DR-1[a]	NKR	0.703047(7)	0.283203(4)	0.513036(4)	18.8538	15.5114	38.5652
SM01-DR-24-14[b]	JM	0.703368(8)	-	0.512910(5)	18.8331	15.5057	38.5979
SM01-DR-23-3[b]	JM	0.703456(6)	0.283088(7)	0.512931(5)	18.8494	15.5070	38.6082
SM01-DR-5-5[b]	JM	0.70343(8)	0.283090(4)	0.512914(5)	18.8149	15.5061	38.5865
SM01-DR-60-43[b]	JM	0.703431(8)	0.283083(4)	0.512918(5)	18.8095	15.5051	38.5795
SM01-DR-100-01[b]	SMR	0.703395(8)	0.283233(5)	0.512978(5)	18.7946	15.4979	38.5077
CGB-2011-D17-2a[a]	SMR	0.703339(6)	0.283265(4)	0.512991(6)	18.7206	15.4949	38.4695
SM01-DR70-1[a]	SMR	0.703391(5)	0.283236(4)	0.512979(4)	18.7409	15.4995	38.4923
SM01-DR67-4[b]	SMR	0.703417(8)	0.283196(4)	0.512983(5)	18.8285	15.5012	38.5407
SM01-DR-91-13[b]	SMR	-	0.283314(5)	-	-	-	-
Subaerial samples (samples from Maaløe *et al.*, 1986):							
JM-192[a]	JM	0.703490(7)	0.283083(4)	0.512880(6)	18.7648	15.5167	38.6121
JM-71[a]	JM	0.703454(6)	0.283068(4)	0.512901(5)	18.8186	15.5170	38.6310
JM-84[a]	JM	0.703453(7)	0.283087(4)	0.512903(6)	18.8404	15.5090	38.6229

* Values in parentheses indicate 2σ uncertainty for the last digit expressed.
** NKR: Northern Kolbeinsey Ridge; JM: Jan Mayen Island; SMR: Southern Mohns Ridge.
[a] $^{206}Pb/^{204}Pb$, $^{207}Pb/^{204}Pb$, $^{208}Pb/^{204}Pb$, $^{176}Hf/^{177}Hf$, and $^{143}Nd/^{144}Nd$ measured by MC-ICP-MS (Nu Plasma HR) at the Ecole Normale Supérieure de Lyon. Strontium isotopes were analysed at the University of Wyoming by MC-ICP-MS (ThermoFinnigan NeptunePlus). See Supplementary Information for further analytical details.
[b] Data measured at Bergen Geoanalytical Facility. $^{87}Sr/^{86}Sr$ measured by thermal ionisation mass spectrometry (Finnigan Mat262). $^{143}Nd/^{144}Nd$, $^{177}Hf/^{176}Hf$, $^{206}Pb/^{204}Pb$, $^{207}Pb/^{204}Pb$, and $^{208}Pb/^{204}Pb$ ratios measured by MC-ICP-MS (ThermoFinnigan Neptune). See Supplementary Information for further analytical details.

Typical Mohns Ridge MORB are characterised by relatively high incompatible element contents and enriched radiogenic isotope values (Schilling *et al.*, 1999; 2005; Elkins *et al.*, 2014), but with relatively high $^{208}Pb/^{204}Pb$ and $^{207}Pb/^{204}Pb$ for a given $^{206}Pb/^{204}Pb$, akin to the so-called DUPAL anomaly observed in the southern oceans (Blichert-Toft *et al.*, 2005). The lavas are further characterised by unusually high ε_{Hf} for a given ε_{Nd} (Blichert-Toft *et al.*, 2005), best explained by ancient garnet in the mantle source, perhaps hosted by SCLM. Such a source could have originated as delaminated Greenland continental lithosphere during rifting of the relatively young Greenland basin. All SMR basaltic glasses analysed here are tholeiitic with geochemistry intermediate between typical Mohns Ridge MORB and lavas from Jan Mayen Island, readily explained as products of straightforward binary mixing between Mohns Ridge-type and Jan Mayen Island-type endmember magmas (Figs. 2, 3, S-1, S-2, Table 1).

Unlike the Mohns Ridge, the Kolbeinsey Ridge is overall characterised by orthogonal spreading at ultraslow rates (18 mm yr^{-1}; Mosar *et al.*, 2002; Dick *et al.*, 2003) and relatively thick ocean crust (7-10 km; Kodaira *et al.*, 1997). The NKR segment has a shallower ridge axis and therefore thicker crust than the neighbouring Middle Kolbeinsey Ridge (MKR). While ultraslow ridges are typically characterised by thin crust, tectonic spreading, and peridotite exposure, those features are not observed in the Jan Mayen region despite ultraslow full-spreading rates of 17-18 mm yr^{-1} (Mosar *et al.*, 2002). Recent bathymetric mapping reveals that the Eggvin Bank in the centre of the NKR, in addition to being anomalously shallow, hosts fresh volcanic deposits indicative of high magma supply (*e.g.,* sheet flows vs. monogenetic cones, a nearly subaerial volcanic edifice constructed atop the eastern axial flank wall, and fresh popping rocks) compared to the ends of the segment (Fig. 1). The large seamount lacks fresh fault scarps, suggesting elevated volcanic activity to maintain its height and cover active axial faulting. Regional bathymetry (Smith and Sandwell, 1997) demonstrates the presence off-axis of shallow seafloor and highly segmented slopes persisting up to 30 km (~3 Ma) off-axis, further supporting a long-lived source of active volcanism. Bathymetry further reveals two parallel axial valleys to the south that both host fresh basalt (Fig. 1). This doubling of ridge axes suggests the segment is immature and can be explained by either active relocation of the segment towards the main, more easterly neovolcanic zone, or by simultaneously active, paired axial valleys as observed in Iceland. Either scenario suggests that NKR axial position is influenced by a long-lived source of enhanced magma supply.

Kolbeinsey Ridge basalts overall have notable depletions in incompatible trace elements and long-lived radiogenic isotope signatures, with high ($^{230}Th/^{238}U$) activity ratios, together suggesting high degrees of melting of a depleted garnet peridotite source (Elkins *et al.*, 2014). The abrupt change in purported mantle composition across the Jan Mayen Fracture Zone has been interpreted to indicate a sharp chemical discontinuity, perhaps reflecting a major mantle flow boundary (Haase *et al.*, 1996) (Fig. 3). Former work identified more enriched isotopic and trace element signatures on the Eggvin Bank and NKR than the MKR, generally attributed to the influence of the Jan Mayen hotspot (Schilling *et al.*, 1999;
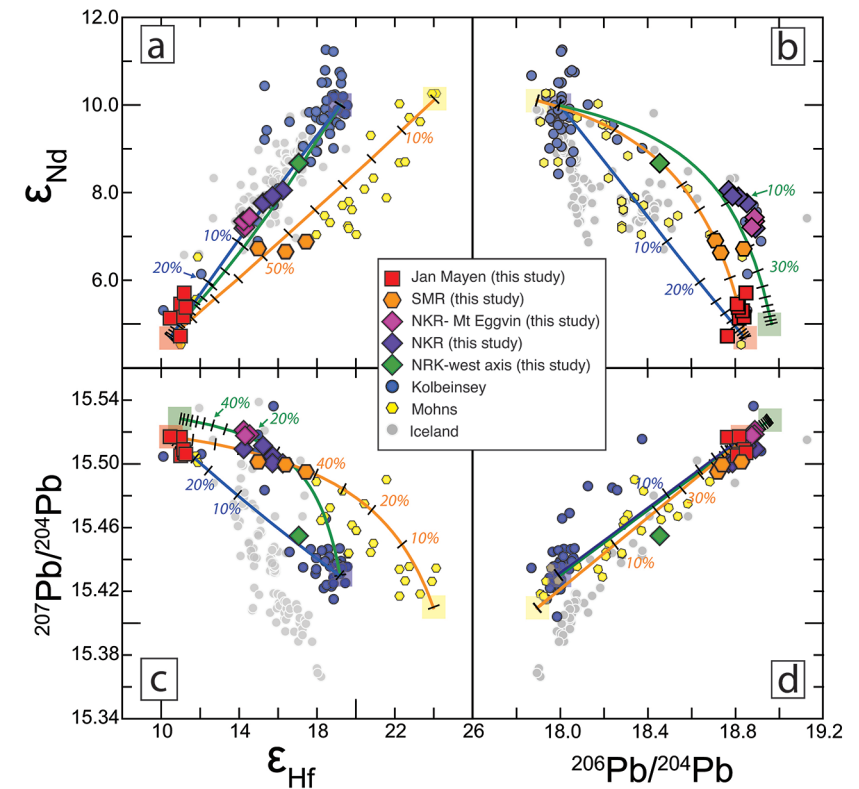
Figure 2 **(a)** ε_{Nd} vs. ε_{Hf}, **(b)** ε_{Nd} vs. $^{206}Pb/^{204}Pb$, **(c)** $^{207}Pb/^{204}Pb$ vs. ε_{Hf}, and **(d)** $^{207}Pb/^{204}Pb$ vs. $^{206}Pb/^{204}Pb$ diagrams for lavas from the Jan Mayen region and Iceland (Sun and Jahn, 1975; Zindler *et al.*, 1979; Óskarsson *et al.*, 1982; Hemond *et al.*, 1993; Nowell *et al.*, 1998; Salters and White, 1998; Schilling *et al.*, 1999; Chauvel and Hémond, 2000; Kempton *et al.*, 2000; Stracke *et al.*, 2003; Blichert-Toft *et al.*, 2005; Elkins *et al.*, 2011; Sims *et al.*, 2013; Elkins *et al.*, 2014) (Tables 1, S-2). Curves show calculated binary mixing trajectories between hypothesised geochemical compositions for Jan Mayen- (red box), Mohns- (yellow), Kolbeinsey- (blue) and Eggvin- (green) type melt endmembers, where tickmarks show percentage contributions of a pure Jan Mayen- or Eggvin-derived magma to a mixture. The Jan Mayen endmember, based on the most extreme enriched measurements for the island (Tables 1, S-2) has ε_{Hf} = +10.5, ε_{Nd} = +4.7, $^{206}Pb/^{204}Pb$ = 18.85, $^{207}Pb/^{204}Pb$ = 15.517, and Hf, Nd, and Pb concentrations of 6.9, 38.7, and 3.7 ppm, respectively. The hypothesised Mohns endmember, extrapolated to values that best explain available SMR samples as binary mixtures of Jan Mayen-Mohns Ridge lavas, has ε_{Hf} = +24, ε_{Nd} = +10.1, $^{206}Pb/^{204}Pb$ = 17.9, $^{207}Pb/^{204}Pb$ = 15.41, and Hf, Nd, and Pb concentrations of 5.6, 30, and 0.7, ppm, respectively; this composition is reasonable compared to published measurements from the Mohns Ridge (Schilling *et al.*, 1999; Schilling *et al.*, 1999; Blichert-Toft *et al.*, 2005; Elkins *et al.*, 2014). The Kolbeinsey endmember, based on depleted values from a suite of published MKR measurements (Schilling *et al.*, 1983; Blichert-Toft *et al.*, 2005; Elkins *et al.*, 2011) and NKR sample POS436 246DR-2, has ε_{Hf} = +19.2, ε_{Nd} = +10, $^{206}Pb/^{204}Pb$ = 18.0, $^{207}Pb/^{204}Pb$ = 15.43, and Hf, Nd, and Pb concentrations of 0.5, 3, and 0.3 ppm, respectively;

mixtures of Jan Mayen and Kolbeinsey endmembers cannot fully explain NKR lava compositions. The Eggvin-type component was extrapolated to values that best explain NKR basalts as mixtures between Kolbeinsey and an unknown enriched component, with ε_{Hf} = +11, ε_{Nd} = +5, $^{206}Pb/^{204}Pb$ = 18.96, $^{207}Pb/^{204}Pb$ = 15.528, $^{208}Pb/^{204}Pb$ = 38.72, and Hf, Nd, and Pb concentrations of 3, 22, and 11 ppm. Note that the high Pb content of the Eggvin-type endmember is necessary to generate a sufficiently hyperbolic mixing trajectory to account for NKR basalts.

Haase *et al.*, 2003; Mertz *et al.*, 2004; Blichert-Toft *et al.*, 2005). Likewise, NKR α_{Sm-Nd} values (where α_{Sm-Nd} = (Sm/Nd)$_{sample}$ / (Sm/Nd)$_{source}$, and (Sm/Nd)$_{source}$ is calculated from $^{143}Nd/^{144}Nd_{sample}$ using a mantle model age of 1.8 Ga; DePaolo, 1988; Sims *et al.*, 1995; Salters, 1996) are more typical of global MORB (<1.0), unlike other Kolbeinsey Ridge basalts with α_{Sm-Nd} > 1.0 (Salters, 1996; Elkins *et al.*, 2011), supporting a distinct mantle source beneath the NKR. While high ($^{230}Th/^{238}U$) activity ratios have suggested melting of a depleted garnet peridotite source for the MKR, NKR lavas have low ($^{231}Pa/^{235}U$) activity ratios, likely the product of rapid melting of garnet-bearing eclogite (Elkins *et al.*, 2011, 2014). We note that the basalt from the eastern axial valley resembles other NKR lavas, including geochemical indicators of enrichment, while the western axial valley basalt more closely resembles MKR basalts and presumably does not sample the enriched mantle component beneath the Eggvin Bank (Figs. 2, 3, S-1, S-2).

While the above observations may suggest plume influence on NKR basalt production, the composition of the enriched endmember in the NKR/Eggvin mantle source differs notably from the Jan Mayen mantle component inferred from Jan Mayen Island- and SMR-derived lavas (Fig. 2). For example, the more enriched basalts collected from the Eggvin Bank exhibit lower (Sm/Yb)$_N$ ratios than the Jan Mayen endmember (Table S-2, Figs. 3, S-1), which cannot be explained by a lack of residual garnet in the source, since NKR magmas are known to be products of melting in the presence of garnet from $^{230}Th/^{238}U$ > 1 (Elkins *et al.*, 2011, 2014). Observed NKR trace element patterns thus likely reflect the composition of a distinct mantle source located beneath the Eggvin Bank. Although not as pronounced as DUPAL-type signatures to the north, this Eggvin-type mantle source also exhibits slightly elevated $^{207}Pb/^{204}Pb$ and $^{208}Pb/^{204}Pb$ ratios for a given $^{206}Pb/^{204}Pb$ and higher ε_{Hf} for a given ε_{Nd} (Table 1, Figs. 2, S-2). Moreover, if generated by binary mixing, the isotopic compositions of Eggvin Bank basalts require a notably Pb-rich Eggvin endmember magma (Fig. 2). In addition to the $^{231}Pa/^{235}U$ evidence for eclogite (Elkins *et al.*, 2014), partition coefficients for Pb, Si, Al, and Fe in eclogite support an eclogite-rich source contributing magmas with the relatively high Pb and SiO_2 and low FeO and Al_2O_3 observed in NKR MORB (Haase *et al.*, 2003; Pertermann and Hirschmann, 2003) (Tables S-2, S-3, Figs. S-2, S-3, S-4). Such an eclogite-bearing source is supported by correlations between Pb and radiogenic isotopes, with higher Pb contents associated with the most enriched isotopic signatures for the NKR (Fig. S-4). We thus infer that the most likely mantle source for the Eggvin-type signature in NKR basalts is an eclogite-rich mantle containing ancient, high-ε_{Hf} garnet (Blichert-Toft *et al.*, 2005). Existing models suggest that garnet-bearing veins or blobs of SCLM are present in the North Atlantic mantle, likely having originated under Greenland
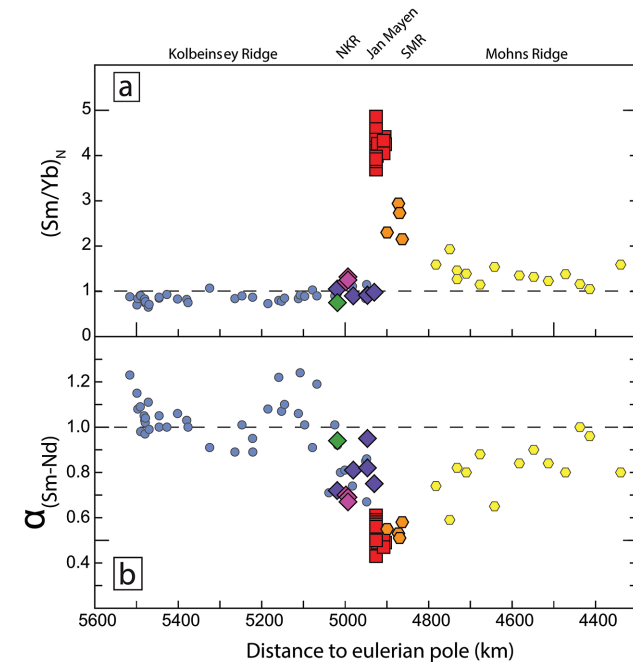
Figure 3 Geochemical indicators vs. along-axis distance for the NKR and SMR, with the position of Jan Mayen Island projected westward onto the NKR using a geographic contour that runs parallel to the Jan Mayen Fracture Zone. **(a)** (Sm/Yb)$_N$, sensitive to the presence of garnet in, and the trace element makeup of, the source. The variation between Jan Mayen Island/SMR and the NKR likely reflects a heterogeneous mantle source. **(b)** α_{Sm-Nd}; because Sm is always more compatible than Nd during melting, values less than unity reflect the degree of melting of the model source, while values greater than unity (*e.g.*, MKR basalts; Salters, 1996; Elkins *et al.*, 2011) require a different source composition and/or younger age than recorded by radiogenic isotopes.

prior to basin rifting by delamination (Blichert-Toft *et al.*, 2005); a concentrated pocket of such material may plausibly have been trapped beneath the NKR by the relocation of the active ridge axis to the Kolbeinsey Ridge from the Aegir Ridge at ~25 Ma (Fig. 1). While the more fusible eclogite can generate thickened crust without elevated mantle temperatures, the other morphological evidence (large near-axis seamounts and paired axial valleys) and extreme nature of the crustal thickening would also support the influence of a plume on mantle temperature beneath the NKR.

The proximity of a small, discrete mantle plume beneath Jan Mayen Island could generate enhanced upwelling and elevated mantle temperatures, producing more melt regionally on both the SMR and NKR. The flow of plume-derived material would likely be directed northward across the fracture zone, influencing

both mantle temperature and basalt composition along the SMR. While a highly fusible eclogite-rich source beneath Jan Mayen is a possibility that cannot be definitively ruled out, the diminishing northward Jan Mayen-type magma signature on the Mohns Ridge is more characteristic of a plume-like point source mixing with adjacent ridge-derived magmas. Any possible Jan Mayen hotspot track is likely confused by the off-axis hotspot location and a local tectonic history of axial relocation, possibly ongoing on the NKR, making the presence of a track unclear. The more fusable, eclogite-bearing, Eggvin-type mantle beneath the NKR could likewise be influenced by the elevated regional temperature anomaly caused by a Jan Mayen plume through the long-term generation of excess magma, although the NKR does not record direct mixing or addition of Jan Mayen-type mantle melts. While we believe this evidence likely favours a small, discrete mantle plume, either scenario results in crustal emplacement of large quantities of magma, producing highly thickened crust, voluminous sheet flows, and a nearly-subaerial (28 m depth), near-axis volcanic seamount.

Jan Mayen and environs demonstrate the dramatic extent to which magmatism generated by heterogeneous mantle, possibly with a plume source, can influence the structure and behaviour of ultraslow mid-ocean ridges. Here, multiple mantle heterogeneities within a relatively small geographic area have significantly modified the accretionary process of two ridge segments, generating enhanced magmatic activity, variations in spreading direction, adjusted axial locations, and, where mantle flow permits, the direct addition of heterogeneous, possibly plume-derived magma. We hence assert that the distinct morphology and tectonically-dominated accretionary style typical of ultraslow spreading ridges (Dick *et al.,* 2003) is particularly sensitive to even modest increases in mantle temperature and magma supply, which cause the ridge to take on growth properties more typical of slow- or intermediate-spreading ridges. For comparison, the 17 °S location on the East Pacific Rise is adjacent to a small hotspot but shows little geomorphological impact at fast spreading rates (Mahoney *et al.,* 1994). This demonstrates that for ultraslow ridges, the control on accretionary mechanisms is principally magma supply, which is typically but, importantly, not solely controlled by spreading rate.

Acknowledgements

Editor: Graham Pearson

Additional Information

Author Contributions

L.J.E. and C.H. conceived and led linked projects, made many of the measurements, and wrote the paper. J.B.T. and S.R.S. made many additional measurements. K.W.W.S. and C.W.D. provided conceptual input and insights and aided in data interpretation. I.A.Y., C.D., and R.P. aided in conceptual input regarding the field area, geomorphology, and sample collection. All authors contributed intellectually and substantively to the paper.

References

BLICHERT-TOFT, J., AGRANIER, A., ANDRES, M., KINGSLEY, R., SCHILLING, J.G., ALBARÈDE, F. (2005) Geochemical segmentation of the Mid-Atlantic Ridge north of Iceland and ridge-hot spot interaction in the North Atlantic. *Geochemistry Geophysics Geosystems* 6, doi: 10.1029/2004GC000788.

CHAUVEL, C., HÉMOND, C. (2000) Melting of a complete section of recycled oceanic crust: Trace element and Pb isotopic evidence from Iceland. *Geochemistry Geophysics Geosystems* 1, 1001.

DEBAILLE, V., TRØNNES, R.G., BRANDON, A.D., WAIGHT, T.E., GRAHAM, D.W., LEE, C.-T.A. (2009) Primitive off-rift basalts from Iceland and Jan Mayen: Os-isotopic evidence for a mantle source containing enriched subcontinental lithosphere. *Geochimica et Cosmochimica Acta* 73, 3423-3449.

DEPAOLO, D. (1988) *Neodymium isotope geochemistry: An introduction.*

DEVEY, C. (2012) *RV Poseidon Cruise Report 436 [POS436]: North Kolbeinsey Ridge - geochemistry and volcanology, 06.07.2012 (Kiel) - 31.07.2012 (Akureyri)*. GEOMAR, Kiel, Germany, doi: 10.3289/CR_POS_436.

DICK, H.J.B., LIN, J., SCHOUTEN, H. (2003) An ultraslow-spreading class of ocean ridge. *Nature* 426, 405-412.

ELKINS, L.J., SIMS, K.W.W., PRYTULAK, J., MATTIELLI, N., ELLIOTT, T., BLICHERT-TOFT, J., BLUSZTAJN, J., DUNBAR, N., DEVEY, C. W., MERTZ, D.F., SCHILLING, J.G. (2011) Understanding melt generation beneath the slow spreading Kolbeinsey Ridge from ^{238}U, ^{230}Th, and ^{231}Pa excesses. *Geochimica et Cosmochimica Acta* 75, 6300-6329.

ELKINS, L.J., SIMS, K.W.W., PRYTULAK, J., BLICHERT-TOFT, J., ELLIOTT, T., BLUSZTAJN, J., FRETZDORFF, S., REAGAN, M., HAASE, K., HUMPHRIS, S., SCHILLING, J.G. (2014) Melt generation beneath Arctic Ridges: Implications from U decay series disequilibria in the Mohns, Knipovich, and Gakkel Ridges. *Geochimica et Cosmochimica Acta* 127, 140-170.

GAINA, C., GERNIGON, L., BALL, P. (2009) Palaeocene-Recent plate boundaries in the NE Atlantic and the formation of the Jan Mayen microcontinent. *Journal of the Geological Society of London* 166, 601-616.

GALE, A., DALTON, C.A., LANGMUIR, C.H., SU, Y., SCHILLING, J.G. (2013) The mean composition of ocean ridge basalts. *Geochemistry Geophysics Geosystems* 14, 489-518.

GALE, A., LANGMUIR, C.H., DALTON, C.A. (2014) The global systematics of ocean ridge basalts and their origin. *Journal of Petrology* 55, 1051-1082.

GÉLI, L., RENARD, V., ROMMEVAUX, C. (2012) Ocean crust formation processes at very slow spreading centers: A model for the Mohns RIdge, near 72°N, based on magnetic, gravity, and seismic data. *Journal of Geophysical Research: Solid Earth* 99, 2995-3013.

HAASE, K.M., DEVEY, C.W., MERTZ, D.F., STOFFERS, P., GARBE-SCHÖNBERG, D. (1996) Geochemistry of lavas from Mohns ridge, Norwegian-Greenland Sea: Implications for melting conditions and magma sources near Jan Mayen. *Contributions to Mineralogy and Petrology* 123, 223-237.

HAASE, K.M., DEVEY, C.W., WIENEKE, M. (2003) Magmatic processes and mantle heterogeneity beneath the slow-spreading northern Kolbeinsey Ridge segment, North Atlantic. *Contributions to Mineralogy and Petrology* 144, 428-448.

HANAN, B.B., BLICHERT-TOFT, J., KINGSLEY, R., SCHILLING, J.G. (2000) Depleted Iceland mantle plume geochemical signature: artifact of multicomponent mixing? *Geochemistry Geophysics Geosystems* 1, doi: 10.1029/1999GC000009.

HEMOND, C., ARNDT, N.T., LICHTENSTEIN, U., HOFMANN, A.W., OSKARSSON, N., STEINTHORSSON, S. (1993) The Heterogeneous Iceland Plume - Nd-Sr-O Isotopes and Trace-Element Constraints. *Journal of Geophysical Research-Solid Earth* 98, 15833-15850.

IMSLAND, P. (1986) The volcanic eruption on Jan Mayen, January 1985: Interaction between a volcanic island and a fracture zone. *Journal of Volcanology and Geothermal Research* 28, 45-53.

JOHNSON, G.L., HEEZEN, B.C. (1967) Arctic Mid-Oceanic Ridge. *Nature* 215, 724-728.

KANDILAROV, A., MJELDE, R., OKINO, K., MURAI, Y. (2008) Crustal structure of the ultra-slow spreading Knipovich Ridge, North Atlantic, along a presumed amagmatic portion of oceanic crustal formation. *Marine Geophysical Researches* 29, 109-134.

KANDILAROV, A., MJELDE, R., PEDERSEN, R.B., HELLEVANG, B., PAPENBERG, C., PETERSEN, C.J., PLANERT, L., FLUEH, E. (2012) The northern boundary of the Jan Mayen microcontinent, North Atlantic determined from ocean bottom seismic, multichannel seismic, and gravity data. *Marine Geophysical Research* 33, 55-76.

KEMPTON, P.D., FITTON, J.G., SAUNDERS, A.D., NOWELL, G.M., TAYLOR, R.N., HARDARSON, B.S., PEARSON, G. (2000) The Iceland plume in space and time: a Sr-Nd-Pb-Hf study of the North Atlantic rifted margin. *Earth and Planetary Science Letters* 177, 255-271.

KLINGELHOFER, F., GÉLI, L., WHITE, R.S. (2000) Geophysical and geochemical constraints on crustal accretion at the very-slow spreading Mohns Ridge. *Geophysical Research Letters* 27, 1547-1550.

KODAIRA, S., MJELDE, R., GUNNARSSON, K., SHIOBARA, H., SHIMAMURA, H. (1997) Crustal structure of the Kolbeinsey Ridge, North Atlantic, obtained by use of ocean bottom seismographs. *Journal of Geophysical Research-Solid Earth* 102, 3131-3151.

LJONES, F., KUWANO, A., MJELDE, R., BREIVIK, A., SHIMAMURA, H., MURAI, Y., NISHIMURA, Y. (2004) Crustal transect from the North Atlantic Knipovich Ridge to the Svalbard margin west of hornsund. *Tectonophysics* 378, 17-41.

MAALØE, S., SØRENSEN, I. B., HERTOGEN, J. (1986) The trachybasaltic suite of Jan Mayen. *Journal of Petrology* 27, 439-466.

MAHONEY, J.J., SINTON, J.M., KURZ, M.D., MACDOUGALL, J.D., SPENCER, K.J., LUGMAIR, G.W. (1994) Isotope and trace element characteristics of a super-fast spreading ridge: East Pacific Rise, 13-23°S. *Earth and Planetary Science Letters* 121, 173-193.

MERTZ, D.F., DEVEY, C.W., TODT, W., STOFFERS, P., HOFMANN, A.W. (1991) Sr-Nd-Pb Isotope Evidence against Plume Asthenosphere Mixing North of Iceland. *Earth and Planetary Science Letters* 107, 243-255.

MERTZ, D.F., SHARP, W.D., HAASE, K.M. (2004) Volcanism on the Eggvin Bank (Central Norwegian-Greenland Sea, latitude similar to 71 degrees N): age, source, and relationship to the Iceland and putative Jan Mayen plumes. *Journal of Geodynamics* 38, 57-83.

MOSAR, J., LEWIS, G., TORSVIK, T.H. (2002) North Atlantic sea-floor spreading rates: implications for the Tertiary development of inversion structures of the Norwegian-Greenland Sea. *Journal of the Geological Society of London* 159, 503-515.

NEUMANN, E.R., SCHILLING, J.G. (1984) Petrology of Basalts from the Mohns-Knipovich Ridge - the Norwegian-Greenland Sea. *Contributions to Mineralogy and Petrology* 85, 209-223.

NOWELL, G.M., KEMPTON, P.D., NOBLE, S.R., FITTON, J.G., SAUNDERS, A.D., MAHONEY, J.J., TAYLOR, R.N. (1998) High precision Hf isotope measurements of MORB and OIB by thermal ionisation mass spectrometry; insights into the depleted mantle. *Chemical Geology* 149, 211-233.

OKINO, K., CUREWITZ, D., ASADA, M., TAMAKI, K., VOGT, P., CRANE, K. (2002) Preliminary analysis of the Knipovich Ridge segmentation: influence of focused magmatism and ridge obliquity on an ultraslow spreading system. *Earth and Planetary Science Letters* 202, 275-288.

ÓSKARSSON, N., SIGVALDASON, G., STEINTHORSSON, S. (1982) A dynamic model of rift zone petrogenesis and the regional petrology of Iceland. *Journal of Petrology* 23, 28-74.

PEDERSEN, R.B., THORSETH, I.H., NYGÅRD, T.E., LILLEY, M.D., KELLEY, D.S. (2010) Hydrothermal activity at the Arctic mid-ocean ridges. In: Rona, P.A., Devey, C.W., Dyment, J., Murton, B.J. (Eds.) *Diversity of Hydrothermal Systems on Slow Spreading Ocean Ridges*. AGU, 67-89.

PERTERMANN, M., HIRSCHMANN, M. (2003) Partial melting experiments on MORB-like pyroxenite between 2 and 3 GPa: Constraints on the presence of pyroxenite in basalt source regions from solidus location and melting rate. *Journal of Geophysical Research* 108, doi: 10.1029/2000JB000118.

SALTERS, V.J.M. (1996) The generation of mid-ocean ridge basalts from the Hf and Nd isotope perspective. *Earth and Planetary Science Letters* 141, 109-123.

SALTERS, V.J.M., WHITE, W.M. (1998) Hf isotope constraints on mantle evolution. *Chemical Geology* 145, 447-460.

SCHILLING, J.G. (1991) Fluxes and excess temperatures of mantle plumes inferred from their interaction with migrating mid-ocean ridges. *Nature* 352, 397-403.

SCHILLING, J.G., ZAJAC, M., EVANS, R., JOHNSTON, T., WHITE, W., DEVINE, J.D., KINGSLEY, R. (1983) Petrologic and Geochemical Variations Along the Mid-Atlantic Ridge from 29-Degrees-N to 73-Degrees-N. *American Journal of Science* 283, 510-586.

SCHILLING, J.G., THOMPSON, G., KINGSLEY, R., HUMPHRIS, S. (1985) Hotspot-migrating ridge interaction in the South Atlantic. *Nature* 313, 187-191.

SCHILLING, J.G., KINGSLEY, R., FONTIGNIE, D., POREDA, R., XUE, S. (1999) Dispersion of the Jan Mayen and Iceland mantle plumes in the Arctic: A He-Pb-Nd-Sr isotope tracer study of basalts from the Kolbeinsey, Mohns, and Knipovich Ridges. *Journal of Geophysical Research-Solid Earth* 104, 10543-10569.

SIMS, K.W.W., DEPAOLO, D.J., MURRELL, M.T., BALDRIDGE, W.S., GOLDSTEIN, S.J., CLAGUE, D.A. (1995) Mechanisms of Magma Generation beneath Hawaii and Midocean Ridges - Uranium/Thorium and Samarium/Neodymium Isotopic Evidence. *Science* 267, 508-512.

SIMS, K.W.W., MACLENNAN, J., BLICHERT-TOFT, J., MERVINE, E. M., BLUSZTAJN, J., GRÖNVOLD, K. (2013) Short length scale mantle heterogeneity beneath Iceland probed by glacial modulation of melting. *Earth and Planetary Science Letters* 379, 146-157.

SMITH, W.H.F., SANDWELL, D.T. (1997) Global sea floor topography from satellite altimetry and ship depth soundings. *Science* 277, 1956-1962.

STRACKE, A., ZINDLER, A., SALTERS, V.J.M., MCKENZIE, D., BLICHERT-TOFT, J., ALBARÈDE, F., GRONVOLD, K. (2003) Theistareykir revisited. *Geochemistry Geophysics Geosystems* 4, doi: 10.1029/2001gc000201.

SUN, S.S., JAHN, B. (1975) Lead and Strontium Isotopes in Postglacial Basalts from Iceland. *Nature* 255, 527-530.

THY, P., LOFGREN, G.E., IMSLAND, P. (1991) Melting relations and the evolution of the Jan Mayen magma system. *Journal of Petrology* 32, 303-332.

TRØNNES, R.G., PLANKE, S., SUNDVOLL, B., IMSLAND, P. (1999) Recent volcanic rocks from Jan Mayen: Low-degree melt fractions of enriched northeast Atlantic mantle. *Journal of Geophysical Research-Solid Earth* 104, 7153-7168.

ZINDLER, A., HART, S.R., FREY, F.A. (1979) Nd and Sr isotope ratios and rare earth element abundances in Reykjanes Peninsula basalts evidence for mantle heterogeneity beneath Iceland. *Earth and Planetary Science Letters* 45, 249-262.

■ North Atlantic hotspot-ridge interaction near Jan Mayen Island

L.J. Elkins[1,2]*, C. Hamelin[3]*, J. Blichert-Toft[4], S.R. Scott[5], K.W.W. Sims[5], I.A. Yeo[6], C.W. Devey[6], R.B. Pedersen[3]

Supplementary Information

The Supplementary Information includes:

➤ Methods

➤ Figures S-1 to S-4

➤ Tables S-1 to S-3

➤ Supplementary Information References

Methods

Submarine NKR, SMR, and Jan Mayen Island samples were retrieved by dredging or ROV sampling on the R/V Poseidon leg 436 (2012), R/V Håkon Mosby leg SM01 (2001), and R/V G.O. Sars leg CGB2011 (2011) (Fig. 1, Table 1), accompanying new high-resolution multibeam bathymetric mapping efforts for targeted sampling of fresh volcanic deposits. Samples were analysed for major and trace element concentrations and $^{87}Sr/^{86}Sr$, $^{143}Nd/^{144}Nd$, $^{176}Hf/^{177}Hf$, $^{206}Pb/^{204}Pb$, $^{207}Pb/^{204}Pb$, and $^{208}Pb/^{204}Pb$ compositions. Glassy submarine samples were handpicked for fresh volcanic glass to avoid visible alteration, palagonite, surface coatings, and phenocrysts. Two of the most primitive (high-MgO) subaerial samples from the Maaløe *et al.* (1986) collection of Beerenberg Volcano on Jan Mayen Island and an additional more evolved (low-MgO) sample were selected for whole rock analysis

1   Department of Geology, Bryn Mawr College, 101 North Merion Avenue, Bryn Mawr, Pennsylvania 19010, USA

2   Department of Earth and Atmospheric Sciences, University of Nebraska Lincoln, Lincoln, NE 68588, USA

3   Center for Geobiology, University of Bergen, Allegaten 41 5007, Bergen, Norway

*   Corresponding and first authors (email: lelkins@unl.edu, Cedric.Hamelin@uib.no)

4   Laboratoire de Géologie de Lyon, Ecole Normale Superieure de Lyon, 46 Allée d'Italie, 69007 Lyon, France

5   Department of Geology and Geophysics, University of Wyoming, Laramie, Wyoming 82071, USA

6   GEOMAR, Helmholtz Center for Ocean Research Kiel, Wischhofstraße 1-3 24148, Kiel, Germany

to compare with submarine samples; major element concentrations of submarine Jan Mayen Island rocks with high crystalline contents were also measured by whole rock analysis. All whole rock material was prepared by hand crushing and grinding to small rock chips using an agate mortar and pestle.

Subaerial, crystalline rock samples JM-192, JM-71, and JM-84 were measured using whole rock analysis of rock chips, following removal of any altered rinds or large phenocrysts. Submarine samples SM01-DR-5-5 and SM01-DR-60-43 contained glassy, fresh groundmass from recent, historic lava flows, and were handpicked to remove any visible surface alteration or large phenocrysts. All other submarine samples were handpicked for pure, fresh, unaltered glass. To remove surface impurities, handpicked samples prepared for trace element and isotopic analysis at the University of Wyoming, the Ecole Normale Supérieure de Lyon, and Boston University were leached with 0.1 % oxalic acid + 2 % H_2O_2 for 15 minutes in an ultrasonic bath, followed by three rinses in ultrapure water, and then leached for an additional 15 minutes in an ultrasonic bath with 0.1 % HCl + 2 % H_2O_2 and again rinsed three times. Handpicked samples prepared at University of Bergen (Tables 1, S-2) were leached for 10 minutes in 1 % H_2O_2 in an ultrasonic bath, followed by three rinses in ultrapure water and then leached briefly in concentrated ultrapure HBr. Whole rock samples were ground to powder or small chips using an agate mortar and pestle for whole rock analysis.

Major elements for glassy samples were determined using an Electron Probe Microanalyzer JXA-8900 at the University of Maryland NanoCenter and the NispLab (Table S-3). For electron probe analysis of major elements, a minimum of 15 points were analysed per sample on one to four homogeneous, handpicked glass chips. For trace element analysis at Boston University, samples were dissolved using a HF-HNO$_3$-HClO$_4$ dissolution procedure and subsequently dried and redissolved in weak HNO$_3$ for analysis by ICP-MS. At the University of Bergen, glass shards were analysed by LA-ICP-MS with a 120 μm diameter beam, pulse frequency of 10 Hz, beam energy of 0.3 mJ/pulse, and total ablation time of 90 s. NIST-glass CaO content (determined by electron microprobe) was used as a calibrating standard, and W-2 and BCR were analysed as unknowns in each sample batch, with accuracies of 2 to 8 % for rare earth elements.

Due to high crystallinity, subaerial samples from Jan Mayen Island were analysed for major elements by whole rock analysis of dissolved rock chips, and two fresh submarine samples dredged from the island's flank were analysed in the same fashion using glassy groundmass hand-picked to remove large phenocrysts. All whole rock chips were then analysed for major elements at Boston University by ICP-AES (Table S-3) using methods after Murray *et al.* (2000). Glass chips for NKR samples and a subsuite of SMR samples and the whole rock chips from Jan Mayen Island described above were further analysed for a full suite of trace element abundances at Boston University (Table S-2) (Murray *et al.*, 2000; Scudder *et al.*, 2014; Dunlea *et al.*, 2015). Handpicked glass chips from the remaining SMR and Jan Mayen Island samples were analysed for major and trace elements in Bergen by laser ablation inductively coupled plasma mass spectrometry (LA-ICP-MS) using a New Wave UP213 laser and a Finnigan Element2 ICP-MS at the University of Bergen (Tables S-2, S-3).

Northern Kolbeinsey Ridge basalt glass chips, a subsuite of SMR (Table S-1) basalt glass chips, and subaerial Jan Mayen Island basalt whole rock chips (see description above) were analysed for $^{143}Nd/^{144}Nd$, $^{176}Hf/^{177}Hf$, $^{206}Pb/^{204}Pb$, $^{207}Pb/^{204}Pb$, and $^{208}Pb/^{204}Pb$ compositions by multi-collector inductively coupled plasma mass spectrometry (MC-ICP-MS) (Nu Plasma 500 HR) at the Ecole Normale Supérieure de Lyon, all on the same sample dissolutions (Table 1). Splits from these same sample dissolutions were analysed for $^{87}Sr/^{86}Sr$ at the University of Wyoming, also by MC-ICP-MS (ThermoFinnigan™ NeptunePlus) (Table 1). Handpicked glass chips from additional SMR and Jan Mayen Island samples were analysed for $^{87}Sr/^{86}Sr$, $^{143}Nd/^{144}Nd$, $^{176}Hf/^{177}Hf$, $^{206}Pb/^{204}Pb$, $^{207}Pb/^{204}Pb$, and $^{208}Pb/^{204}Pb$ compositions at the University of Bergen (Table 1); $^{87}Sr/^{86}Sr$ was analysed by thermal ionisation mass spectrometry (TIMS) (Finnigan Mat262) and $^{143}Nd/^{144}Nd$, $^{176}Hf/^{177}Hf$, $^{206}Pb/^{204}Pb$, $^{207}Pb/^{204}Pb$, and $^{208}Pb/^{204}Pb$ compositions were measured by MC-ICP-MS (ThermoFinnigan™ Neptune). Additional methods details provided in Supplementary Information.

$^{206}Pb/^{204}Pb$, $^{207}Pb/^{204}Pb$, $^{208}Pb/^{204}Pb$, $^{176}Hf/^{177}Hf$, and $^{143}Nd/^{144}Nd$ isotope compositions measured by MC-ICP-MS in Lyon were analysed following the procedures in Blichert-Toft and Albarède (2009) with the exception that Ln-Spec instead of HDEHP columns were used for Nd purification. Hafnium and Nd were normalised for instrumental mass bias relative to $^{179}Hf/^{177}Hf = 0.7325$ and $^{146}Nd/^{144}Nd = 0.7219$, respectively. $^{176}Hf/^{177}Hf$ of the JMC-475 Hf standard = 0.282160 ± 0.000010 (n = 45), and $^{143}Nd/^{144}Nd$ of the Rennes in-house standard = 0.511961 ± 0.000013 (n = 45) (Chauvel and Blichert-Toft, 2001). Pb isotope compositions were analysed using Tl doping and sample-standard bracketing and the values of Eisele *et al.* (2003) for NIST 981. External reproducibilities of $^{206}Pb/^{204}Pb$, $^{207}Pb/^{204}Pb$, and $^{208}Pb/^{204}Pb$ are 100-200 ppm or 0.01-0.02 %. Hf, Nd, and Pb total procedural blanks were <20 pg.

Following partial separation in Lyon from the same sample dissolutions used for Hf, Nd, and Pb isotope work, Sr was purified at the University of Wyoming using cation-exchange resin in HCl followed by a Sr-Spec column to remove Rb. $^{87}Sr/^{86}Sr$ compositions were analysed using a ThermoFinnigan™ NeptunePlus MC-ICP-MS instrument with an Apex desolvating nebuliser. Strontium isotopes were analysed in static mode, using four Faraday collectors with ratios normalised to $^{86}Sr/^{88}Sr = 0.1194$ to account for instrumental mass bias. Additional Faraday collectors were used to monitor Rb and Kr interferences, which were nearly undetectable at <0.0002 volts for ^{83}Kr and ≤0.0001 volts for ^{85}Rb in all analyses; any Kr interferences detected using the ^{83}Kr peak were then corrected using natural abundances. Strontium isotope ratios are reported relative to NBS987 $^{87}Sr/^{86}Sr = 0.71024$. Total procedural blanks for Sr were <100 pg, and external reproducibility of $^{87}Sr/^{86}Sr$ for BCR-2 and other rock standards is ~ ±0.000016 (2σ).

At the University of Bergen Geoanalytical Facility, handpicked glass chips were dissolved in concentrated HF + HBr. Lead was extracted using methods after Manhes *et al.* (1978) and Sr, Nd, and Hf after Hamelin *et al.* (2013). $^{87}Sr/^{86}Sr$ was measured using a Finnigan Mat262 TIMS at the University of Bergen and $^{143}Nd/^{144}Nd$, $^{176}Hf/^{177}Hf$, $^{206}Pb/^{204}Pb$, $^{207}Pb/^{204}Pb$, and $^{208}Pb/^{204}Pb$ compositions were measured using a ThermoFinnigan Neptune MC-ICP-MS. Repeated

measurements of international standard solutions during analyses yielded $^{87}Sr/^{86}Sr = 0.710238 \pm 8$ (n = 4, 2σ) for the NBS987 Sr standard, $^{143}Nd/^{144}Nd = 0.511845 \pm 6$ (n = 13, 2σ) for the LaJolla Nd standard, $^{177}Hf/^{176}Hf = 0.282148\pm3$ (n = 15, 2σ) for the JMC-475 Hf standard, and $^{206}Pb/^{204}Pb = 16.9351 \pm 13$ (n = 8, 2σ), $^{207}Pb/^{204}Pb = 15.4889 \pm 14$ (n = 8, 2σ), and $^{208}Pb/^{204}Pb = 36.6879 \pm 37$ (n = 8, 2σ) for the NBS981 Pb standard. Instrumental mass fractionation of Pb was corrected for using the Tl doping and sample-standard bracketing technique. Data in Table 1 are reported relative to the following standard values: $^{87}Sr/^{86}Sr = 0.71024$, $^{143}Nd/^{144}Nd = 0.511856$, $^{177}Hf/^{176}Hf = 0.282157$, $^{206}Pb/^{204}Pb = 16.9371$, $^{207}Pb/^{204}Pb = 15.4913$, and $^{208}Pb/^{204}Pb = 36.7213$.

Supplementary Figures
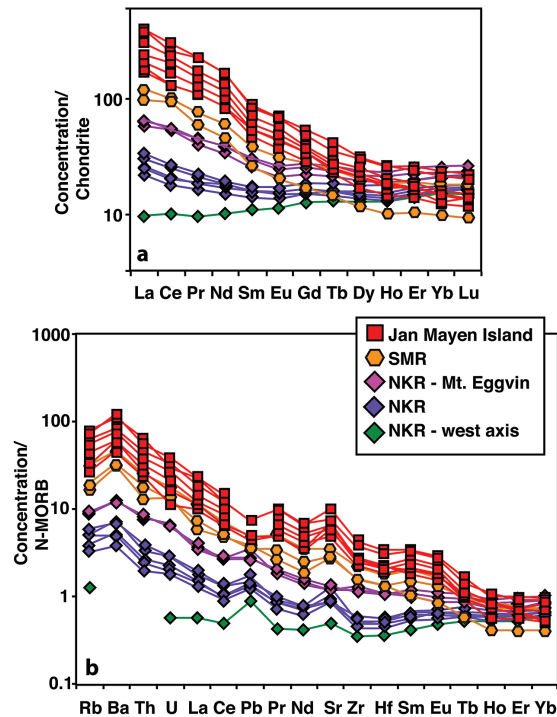
Figure S-1 **(a)** Chondrite-normalised (McDonough and Sun, 1995) REE concentrations and **(b)** N-MORB (Hofmann, 1988) normalised trace element concentrations for samples from this study (Table S-2). NKR basalts have elevated Pb and HREE compared to Jan Mayen Island and the MKR, indicating that they cannot be simple mixtures of Kolbeinsey-type and Jan Mayen-type magmas. High ($^{230}Th/^{238}U$) ratios measured in NKR lavas also require the presence of garnet in the melt source, indicating that the trace element compositions in Eggvin Bank basalts is principally controlled by mantle source composition.
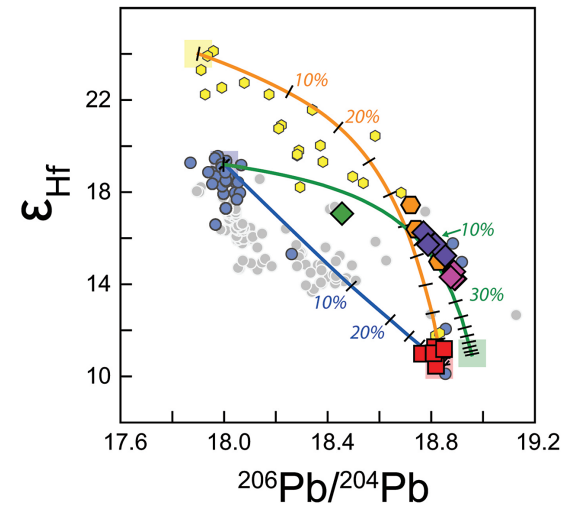
Figure S-2 $ε_{Hf}$ vs. $^{206}Pb/^{204}Pb$ for the Jan Mayen region, with symbols, mixing trajectories, and references as in Figure 2.
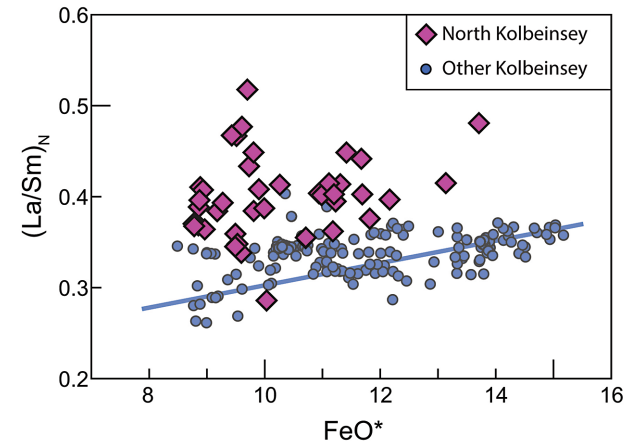
Figure S-3 $(La/Sm)_N$ vs. FeO* for basalt samples from the Kolbeinsey Ridge and the NKR, using data from Haase *et al.* (2003) and C. Devey, M. Wieneke, and K. Haase (unpub. data). Linear best-fit regression for Kolbeinsey Ridge samples suggests a slight positive relationship between FeO* and $(La/Sm)_N$, likely controlled by degree of melting. Basalt rocks from the NKR are restricted to generally higher $(La/Sm)_N$ and lower FeO* values than the rest of the Kolbeinsey Ridge, best explained by an eclogite-bearing, incompatible element-enriched mantle source beneath the Eggvin Bank.
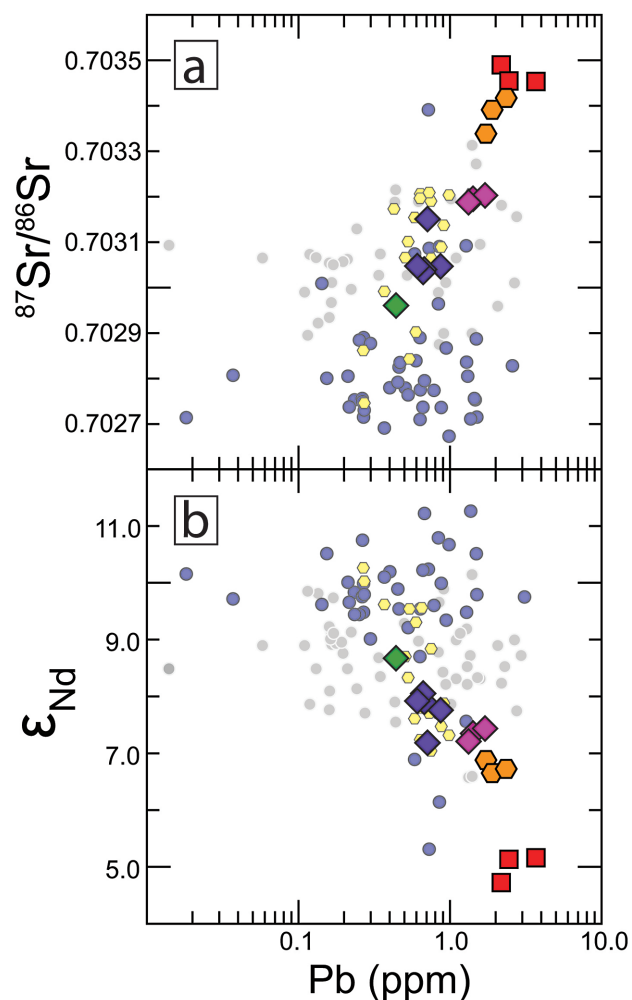
Figure S-4 **(a)** $^{87}Sr/^{86}Sr$ vs. Pb, and **(b)** ε_{Nd} vs. Pb. for the Jan Mayen region, with symbols and references as in Figure 2. The data support lithologically and isotopically heterogeneous mantle source compositions for the Jan Mayen region and corroborate the existence of an Eggvin Bank end-member distinct from Jan Mayen mantle.

Supplementary Tables

Table S-1 Location information for new submarine samples analysed in this study.

Sample number*	Location	Expedition[b]	Year	Latitude (°N)		Longitude (°W)		Depth (m)	
				Start	Stop	Start	Stop	Start	Stop
POS436 242DR-2b	NKR	R/V Poseidon Leg 436	2012	70.7600	70.7650	13.5504	13.5448	1559	1436
POS436 246DR-2	NKR	R/V Poseidon Leg 436	2012	70.7894	70.7947	13.7535	13.7540	1714	1630
POS436 235DR-1a	NKR	R/V Poseidon Leg 436	2012	70.9128	70.9124	13.1241	13.1125	485	381
POS436 253DR-E2	NKR	R/V Poseidon Leg 436	2012	70.9490	70.9474	13.0348	13.0377	207	175
POS436 253DR-6	NKR	R/V Poseidon Leg 436	2012	70.9490	70.9474	13.0348	13.0377	207	175
POS436 232DR-1	NKR	R/V Poseidon Leg 436	2012	71.0599	71.0566	12.9523	12.9398	622	578
POS436 209DR-2a	NKR	R/V Poseidon Leg 436	2012	71.3134	71.3159	12.7027	12.6945	1199	1205
POS436 222DR-1	NKR	R/V Poseidon Leg 436	2012	71.3470	71.3472	12.6433	12.6293	1139	1137
POS436 215DR-1	NKR	R/V Poseidon Leg 436	2012	71.4766	71.4760	12.3938	12.4062	1819	1703
SM01-DR-24-14[a]	JM	R/V Håkon Mosby, SM01	2001	-	71.1287	-	7.8082	-	738
SM01-DR-23-3	JM	R/V Håkon Mosby, SM01	2001	-	71.1022	-	7.7913	-	697
SM01-DR-5-5	JM	R/V Håkon Mosby, SM01	2001	-	71.1192	-	7.9187	-	47
SM01-DR-60-43	JM	R/V Håkon Mosby, SM01	2001	-	71.1645	-	7.9880	-	222
SM01-DR-100-01	SMR	R/V Håkon Mosby, SM01	2001		70.9855	-	6.4003	-	2493
CGB-2011-D17-2a	SMR	R/V G.O. Sars, CGB2011	2011	71.2617	71.2613	5.8430	5.8397	-	847
SM01-DR70-1	SMR	R/V Håkon Mosby, SM01	2001	-	71.2382	-	6.1102	-	953
SM01-DR67-4	SMR	R/V Håkon Mosby, SM01	2001	-	71.2188	-	6.1713	-	806
SM01-DR-91-13	SMR	R/V Håkon Mosby, SM01	2001	-	71.2715	-	5.8468	-	732

* All samples collected by dredge, except ROV dive sample CGB-2011-D17-2a. For SM01 cruise, only end locations for dredges were recorded.
[a] SM01 and CGB-2011 sample depths are calculated from GEBCO global bathymetry (IOC, IHO, BODC, 2003).
[b] R/V Poseidon sample information available in Earthchem/IEDA database (Elkins, 2015).

Table S-2   Trace element abundance measured by ICP-MS.

Sample	Location	Li	Sc	V	Cr	Co	Ni	Cu	Zn	Rb	Sr	Zr	Y	Mo	Ba	La
Submarine samples:																
POS436 242DR-2b[a]	NKR	4.9	47.8	274.7	404.1	45.6	127.1	88.0	79.2	7.5	145.5	54.8	24.7	0.5	99.0	8.0
POS436 246DR-2[a]	NKR	4.5	46.9	275.3	246.0	49.4	85.7	110.2	72.4	1.6	56.4	36.5	23.9	0.2	-	2.3
POS436 235DR-1a[a]	NKR	7.7	43.7	424.4	18.1	43.8	20.1	49.9	104.2	12.0	150.0	118.6	39.6	0.9	172.2	15.4
POS436 253DR-E2[a]	NKR	6.8	36.9	409.0	14.6	42.9	174.6	49.1	105.8	11.6	140.4	128.2	34.6	1.0	175.7	15.1
POS436 253DR-6[a]	NKR	6.6	30.2	402.3	19.4	43.2	38.8	73.8	160.4	11.4	138.1	132.4	32.6	1.2	173.2	13.7
POS436 232DR-1[a]	NKR	4.9	47.9	280.4	376.3	46.2	106.3	92.3	73.8	4.2	99.2	46.8	25.5	0.4	52.7	5.2
POS436 209DR-2a[a]	NKR	6.7	52.9	329.2	173.9	47.6	55.7	77.4	89.9	6.4	103.2	52.4	33.2	0.4	66.4	5.8
POS436 222DR-1[a]	NKR	5.5	47.4	302.1	226.0	47.0	74.3	88.4	83.2	4.8	110.3	50.6	27.7	0.5	72.3	6.0
POS436 222DR-1 replicate[a]	NKR	5.4	49.2	311.1	233.2	48.5	74.4	91.6	87.3	5.2	114.6	52.7	28.6	0.5	75.1	6.2
POS436 215DR-1[a]	NKR	5.8	38.3	332.2	87.6	47.4	51.6	76.0	98.7	6.6	100.1	61.8	25.6	0.6	103.4	7.2
SM01-DR-24-14[b]	JM	-	-	-	17.0	-	31.8	-	-	76.8	764.4	285.5	31.3	-	1192.4	71.6
SM01-DR-23-3[b]	JM	-	-	-	3.7	-	-	-	-	90.5	876.6	404.6	39.6	-	1727.2	94.9
SM01-DR-5-5[b]	JM	-	-	-	39.2	-	23.2	-	-	54.6	556.9	231.9	26.8	-	832.2	48.6
SM01-DR-60-43[b]	JM	-	-	-	20.0	-	22.8	-	-	69.7	674.7	261.5	28.7	-	1051.6	56.5
SM01-DR-100-01[b]	SMR	-	-	-	7.6	-	29.8	-	-	29.4	315.9	173.2	32.8	-	454.7	0.0
CGB-2011-D17-2a[a]	SMR	6.3	31.4	367.8	23.4	41.8	28.3	54.8	103.8	24.5	326.2	162.1	30.8	2.0	453.7	28.8
SM01-DR70-1[a]	SMR	4.0	18.3	361.5	24.4	42.2	33.5	63.9	95.3	20.9	316.8	165.1	19.3	2.1	423.8	23.2
SM01-DR67-4[a]	SMR	7.0	25.4	423.8	26.9	44.4	22.3	55.5	107.6	39.7	403.5	227.6	30.4	-	639.1	45.0
SM01-DR-91-13[b]	SMR	-	-	-	9.0	-	15.5	-	-	21.0	244.6	135.1	32.5	-	319.3	20.3
Subaerial samples (samples from Maaløe et al., 1986):																
JM-192[a]	JM	5.1	40.4	284.7	671.1	49.6	167.5	34.0	87.1	33.0	820.8	279.2	30.5	1.8	620.1	40.5
JM-71[a]	JM	4.8	35.3	364.3	533.0	51.9	188.1	100.0	81.4	41.6	650.7	287.5	25.3	2.3	814.7	44.1
JM-84[a]	JM	7.7	27.1	347.7	55.9	33.9	38.6	51.9	102.8	101.8	1156.9	457.5	46.0	4.0	1546.7	90.8
Rock standard:																
BHVO-2		4.4	29.1	315.3	327.6	48.4	122.9	132.2	104.0	8.0	365.8	158.7	24.5	-	128.8	14.6

Sample	Ce	Pr	Nd	Sm	Eu	Gd	Tb	Dy	Ho	Er	Yb	Lu	Hf	Pb	U	Th
Submarine samples:																
POS436 242DR-2b[a]	16.3	2.1	8.9	2.3	0.8	3.0	0.5	3.4	0.7	2.3	2.5	0.4	1.5	0.7	0.21	0.76
POS436 246DR-2[a]	6.1	0.9	4.6	1.6	0.6	2.5	0.5	3.1	0.7	2.2	2.4	0.4	1.1	0.4	0.04	-
POS436 235DR-1a[a]	33.0	4.2	17.8	4.5	1.5	5.4	0.9	5.9	1.3	4.0	4.1	0.6	3.1	1.3	0.44	1.60
POS436 253DR-E2[a]	34.4	4.1	17.4	4.3	1.4	5.0	0.9	5.4	1.1	3.6	3.7	0.6	3.4	1.4	0.49	1.54
POS436 253DR-6[a]	32.4	3.7	15.3	3.7	1.2	4.4	0.8	4.7	1.0	3.2	3.3	0.5	3.3	1.7	0.48	1.49
POS436 232DR-1[a]	11.0	1.5	7.0	2.1	0.8	2.9	0.5	3.5	0.8	2.4	2.6	0.4	1.4	0.6	0.13	0.37
POS436 209DR-2a[a]	12.3	1.7	8.1	2.6	0.9	3.7	0.7	4.4	1.0	3.1	3.4	0.5	1.6	0.7	0.14	0.46
POS436 222DR-1[a]	12.7	1.7	7.8	2.3	0.9	3.3	0.6	3.9	0.8	2.7	2.8	0.4	1.5	0.7	0.16	0.50
POS436 222DR-1 replicate[a]	12.9	1.8	8.1	2.4	0.9	3.3	0.6	3.9	0.9	2.7	2.9	0.4	1.5	0.7	0.16	0.54
POS436 215DR-1[a]	15.4	2.0	8.5	2.3	0.8	3.1	0.6	3.7	0.8	2.5	2.7	0.4	1.7	0.9	0.21	0.62
SM01-DR-24-14[b]	144.2	16.2	60.1	10.2	3.1	7.8	1.0	6.1	1.1	3.0	2.6	0.4	6.5	-	2.31	8.56
SM01-DR-23-3[b]	184.6	20.9	75.4	12.3	3.8	9.6	1.3	7.4	1.4	3.9	3.4	0.5	9.1	-	2.75	10.39
SM01-DR-5-5[b]	100.9	11.9	45.3	8.0	2.4	6.8	0.9	5.2	1.0	2.6	2.1	0.3	5.7	-	1.46	5.97
SM01-DR-60-43[b]	123.2	14.0	52.7	9.0	2.8	7.3	1.0	5.5	1.0	2.7	2.3	0.3	6.2	-	1.91	7.34
SM01-DR-100-01[b]	65.1	8.2	31.4	6.2	2.0	5.6	0.8	5.4	1.1	3.0	3.0	0.4	4.0	-	0.95	0.95
CGB-2011-D17-2a[a]	60.9	7.1	27.7	5.7	1.8	5.6	0.9	5.0	1.0	3.0	3.0	0.5	4.0	1.7	0.93	3.44
SM01-DR70-1[a]	58.0	5.6	21.3	3.9	1.2	3.4	0.5	2.9	0.6	1.7	1.6	0.2	4.0	1.9	0.99	2.46
SM01-DR67-4[a]	85.5	10.7	39.8	7.6	2.2	6.7	1.0	5.9	1.1	3.2	2.9	0.4	5.3	2.4	4.86	1.29
SM01-DR-91-13[b]	45.3	5.7	23.6	5.5	1.8	5.5	0.8	5.6	1.2	3.3	3.3	0.5	3.6	-	0.64	2.44
Subaerial samples:																
JM-192[a]	78.8	10.1	39.5	7.7	2.5	6.8	1.0	5.1	0.9	2.7	2.3	0.3	6.9	2.2	0.81	4.45
JM-71[a]	80.1	10.1	37.9	6.9	2.1	5.7	0.8	4.2	0.8	2.2	2.0	0.3	6.9	2.5	1.14	5.08
JM-84[a]	154.6	20.8	76.2	13.1	3.9	10.6	1.5	7.7	1.4	4.1	3.7	0.5	10.4	3.7	2.06	12.22
Rock standard:																
BHVO-2	36.1	5.4	23.8	6.0	2.0	5.9	0.9	5.2	0.9	2.4	1.9	0.3	4.3	1.6	1.23	0.41

[a] Trace elements measured by ICP-MS (VG Plasma Quad ExCell) at Boston University, with 1-2 % standard deviations.
[b] Trace elements measured by LA-ICP-MS (Thermo-Finnigan Element2) at the University of Bergen, with 2-5 % standard deviations.

Table S-3 Major element composition results.

Sample	Location	SiO2	Al2O3	TiO2	CaO	MnO	MgO	FeO	Fe2O3	Na2O	K2O	Cr2O3	P2O5	Cl	Total
Submarine samples:															
POS436 242DR-2b	NKR	50.69(8)	15.25(4)	1.04(2)	13.02(4)	-	8.37(5)	8.66(5)	-	1.70(1)	0.267(4)	0.09(1)	0.144(7)	0.032(2)	99.4(1)
POS436 246DR-2	NKR	50.73(9)	15.02(4)	0.85(3)	13.64(6)	-	8.95(3)	9.16(7)	-	1.57(1)	0.074(3)	0.07(1)	0.094(7)	0.012(1)	100.3(1)
POS436 235DR-1a	NKR	52.27(9)	13.06(4)	2.25(5)	8.68(5)	-	4.54(3)	14.60(6)	-	2.76(2)	0.551(4)	0.031(9)	0.22(1)	0.141(3)	99.3(2)
POS436 253DR-E2	NKR	52.5(2)	11.9(9)	2.0(1)	9.8(6)	-	6.2(1.3)	13.6(2)	-	2.5(3)	0.45(5)	0.03(1)	0.20(2)	0.14(2)	99.5(2)
POS436 253DR-6	NKR	52.70(8)	12.8(5)	2.06(7)	9.1(2)	-	5.4(7)	13.66(7)	-	2.7(1)	0.50(3)	0.034(9)	0.22(1)	0.149(8)	99.5(2)
POS436 232DR-1	NKR	50.90(7)	14.83(3)	1.00(3)	13.16(5)	-	8.30(3)	9.30(6)	-	1.777(9)	0.192(2)	0.07(1)	0.074(5)	0.028(1)	99.8(1)
POS436 209DR-2a	NKR	52.2(1)	13.03(4)	2.28(3)	8.68(3)	-	4.57(2)	14.70(7)	-	2.75(2)	0.568(2)	0.05(1)	0.233(8)	0.143(2)	99.4(2)
POS436 222DR-1	NKR	51.4(1)	14.58(4)	1.10(2)	12.44(5)	-	7.56(7)	10.22(5)	-	1.95(3)	0.230(3)	0.06(1)	0.095(7)	0.026(1)	99.9(1)
POS436 215DR-1	NKR	52.24(7)	14.24(4)	1.25(3)	11.09(6)	-	6.64(3)	11.50(7)	-	2.088(8)	0.309(3)	0.027(7)	0.121(8)	0.038(2)	99.7(1)
SM01-DR-24-14	JM	47.8(1)	15.11(4)	4.42(3)	8.94(6)	-	3.70(2)	12.20(6)	-	3.26(2)	3.10(5)	0.009(5)	0.75(1)	0.118(3)	99.6(2)
SM01-DR-23-3	JM	56.8(1)	17.14(4)	2.14(4)	4.56(4)	-	2.19(1)	6.11(4)	-	3.7(2)	3.93(2)	0.020(6)	0.453(8)	0.191(3)	97.5(2)
SM01-DR-5-5[a]	JM	48.01	15.1908	3.29	10.31	0.20	6.45	-	12.1	2.98	2.48	-	0.59	0.06	101.7
SM01-DR-60-43[a]	JM	48.17	16.1320	3.51	10.41	0.20	5.05	-	12.8	3.02	2.67	-	0.62	0.12	102.7
CGB-2011-D17-2a	SMR	51.4(2)	14.57(7)	2.44(2)	9.77(6)	-	5.22(2)	11.57(7)	-	2.90(1)	1.003(8)	0.015(7)	0.367(9)	0.152(2)	99.6(3)
SM01-DR70-1	SMR	50.37(7)	14.74(4)	2.37(3)	10.17(5)	-	5.62(2)	10.5(1)	-	2.75(2)	0.984(6)	0.026(9)	0.354(8)	0.124(2)	98.2(2)
SM01-DR67-4	SMR	51.18(9)	14.35(8)	2.86(3)	9.08(4)	-	4.61(3)	11.06(9)	-	2.85(4)	1.40(3)	0.029(9)	0.476(9)	0.109(3)	98.2(2)
SM01-DR-91-13	SMR	52.1(2)	14.17(4)	2.34(3)	9.8(2)	-	5.2(1)	12.0(1)	-	2.5(2)	0.75(1)	0.025(7)	0.298(8)	0.069(2)	99.4(2)
Subaerial samples (samples from Maaløe _et al._, 1986):															
JM-192[a]	JM	47.39	12.92	2.52	12.45	0.17	11.13	-	11.1	2.20	1.13	-	0.43	-	101.4
JM-71[a]	JM	46.41	12.84	2.48	12.11	0.17	10.61	-	11.0	2.16	1.15	-	0.42	-	99.3
JM-84[a]	JM	47.65	16.52	3.26	9.88	0.19	5.02	-	11.1	3.59	2.05	-	0.68	-	100.0
Rock standard:															
BHVO-2		48.80	13.30	2.74	11.20	0.16	7.17	-	12.1	2.11	0.50	-	0.27	-	98.4

* Major element concentrations of glass chips measured by EPMA methods unless otherwise indicated. EPMA results report uncertainties expressed in parentheses as 1s standard error for the last digit reported. Values shown are mean values of at least 15 analysed points. measured using a 20 keV beam. All Fe measured as FeO.
[a] Whole rock chips analysed for major element concentrations by ICP-ES (Jobin-Yovn Ultima-C) with standard deviations of 1-2 %. All Fe measured as Fe_2O_3.

Supplementary Information References

Blichert-Toft, J., Albarède, F. (2009) Mixing of isotopic heterogeneities in the Mauna Kea plume conduit. _Earth and Planetary Science Letters_ 282, 190-200.

Chauvel, C., Blichert-Toft, J. (2001) A hafnium isotope and trace element perspective on melting of the depleted mantle. _Earth and Planetary Science Letters_ 190, 137-151.

Dunlea, A.G., Murray, R.W., Sauvage, J., Spivack, A.J., Harris, R.N., D'Hondt, S. (2015) Dust, volcanic ash, and the evolution of the South Pacific Gyre through the Cenozoic. _Palaeoceanography_, doi: 10.1002/2015PA002829.

Eisele, J., Abouchami, W., Galer, S.J.G., Hofmann, A.W. (2003) The 320 kyr Pb isotope evolution of Mauna Kea lavas recorded in teh HSDP-2 drill core. _Geochemistry Geophysics Geosystems_ 4, 8710.

Elkins, L.J. (2015) Jan Mayen glass and whole rock chemistry. _IEDA/Earthchem data set_, doi: 10.1594/IEDA/100536.

Haase, K.M., Devey, C.W., Wieneke, M. (2003) Magmatic processes and mantle heterogeneity beneath the slow-spreading northern Kolbeinsey Ridge segment, North Atlantic. _Contributions to Mineralogy and Petrology_ 144, 428-448.

Hamelin, C., Bezos, A., Dosso, L., Escartin, J., Cannat, M., Mevel, C. (2013) Atypically depleted upper mantle component revealed by Hf isotopes at Lucky Strike segment. _Chemical Geology_ 341, 128-139.

Hofmann, A.W. (1988) Chemical differentiation of the Earth: the relationship between mantle, continental crust, and oceanic crust. _Earth and Planetary Science Letters_ 90, 297-314.

IOC, IHO, BODC (2003) _Centenary Edition of the GEBCO Digital Atlas, published on CD-ROM on behalf of the Intergovernmental Oceanographic Commission and the International Hydrographic Organization as part of the General Bathymetric Chart of the Oceans_, Liverpool, UK.

Maaløe, S., Sørensen, I.B., Hertogen, J. (1986) The trachybasaltic suite of Jan Mayen. _Journal of Petrology_ 27, 439-466.

Manhes, G., Minster, J.F., Allègre, C.J. (1978) Comparative uranium-thorium-lead and rubidium-strontium study of Saint Sèverin amphoterite: consequences for early solar system chronology. _Earth and Planetary Science Letters_ 39, 14-24.

McDonough, W.F., Sun, S.S. (1995) The composition of the Earth. _Chemical Geology_ 120, 223-253.

Murray, R.W., Miller, D.J., Kryc, K. (2000) Analysis of major and trace elements in rocks, sediments, and interstitial waters by inductively coupled plasma-atomic emission spectrometry (ICP-AES). _Ocean Drilling Program Technical Note_ 29, 1-27.

Scudder, R.P., Murray, R.W., Schindlbeck, J.C., Kutterolf, S., Hauff, F., McKinley, C.C. (2014) Regional-scale input of dispersed and discrete volcanic ash to the Izu-Bonin and Mariana subduction zones. _Geochemistry Geophysics Geosystems_ 15, 4369-4379.